Article:
Shamsa, A, Barmatov, E, Hughes, TL et al. (3 more authors) (2022) Hydrolysis of imidazoline based corrosion inhibitor and effects on inhibition performance of X65 steel in CO2 saturated brine. Journal of Petroleum Science and Engineering, 208 (Part B). 109235. ISSN 0920-4105

https://doi.org/10.1016/j.petrol.2021.109235

Hydrolysis of imidazoline based corrosion inhibitor and effects on inhibition performance of X65 steel in CO_2 saturated brine

Amir Shamsa[a], Evgeny Barmatov[b], Trevor L. Hughes[b], Yong Hua[a], Anne Neville[a], Richard Barker[a]

[a] Institute of Functional Surface, School of Mechanical Engineering, University of Leeds, Leeds, LS2 9JT, UK

[b] Schlumberger Cambridge Research, Cambridge, CB3 0EL, UK

Abstract

The molecular characteristics of a TOFA/DETA based imidazoline inhibitor were evaluated by analysing the inhibitor protonation profile, the CMC and micelle size and the rate of acid-catalysed hydrolysis of the inhibitor to improve understanding of the corrosion inhibition performance of the main imidazoline component and its hydrolysis products. The ability of the TOFA/DETA imidazoline based corrosion inhibitor and its products of hydrolysis in retarding both uniform and localised corrosion were assessed and compared on wet-ground X65 carbon steel at 80°C in CO2 saturated 3 wt. % NaCl brines. The findings indicate that the imidazoline based inhibitor forms micellar solutions, with a characteristic micelle size of 18±9 nm at the CMC (10±1 ppm) in CO2 saturated 3 wt. % NaCl brines, and that under such conditions (pH~4.1), the inhibitor is fully protonated which increases inhibitor solubility/dispersibility and enhances molecular adsorption of the positively charged imidazoline on the metal surface thereby improving inhibition performance. Hydrolysis of the imidazoline and amido-amine is acid-catalysed and the consumption of imidazoline follows a pseudo-first-order reaction mechanism with an activation energy of 72.0±2.9 kJ mol-1. The study concludes that the pre-aged inhibitor has different effects on uniform and localised corrosion behaviour of X65 carbon steel.

Key words: CO_2 corrosion, imidazoline inhibitor, hydrolysis, localized corrosion

1.0 Introduction

Carbon dioxide (CO_2) enhanced corrosion of carbon steels is an important issue in most stages of oil and gas production. Several methods, including coatings and fluid-mediated corrosion inhibitors are widely used to protect downhole equipment, surface equipment and the hardware used in processing and transport. Typically, commercial corrosion inhibitor formulations used in CO_2 saturated oilfield brines (pH 3-5, 3-5 wt. % NaCl) are based on imidazolines and amido-amines (example structures 1 and 2 are shown in Fig. 1). Such formulations provide effective inhibition due to their strong adsorption and film-forming characteristics and their tolerance to high temperature and dynamic flow conditions.

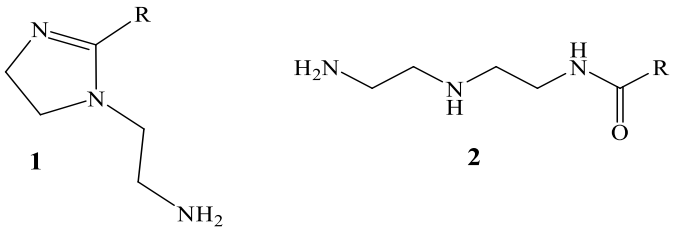

Figure 1: The main components of a commercial imidazoline corrosion inhibitor based on the reaction of diethylene triamine (DETA) and tall oil fatty acid (TOFA): imidazoline **1** and amido-amine **2**.

Alkyl aminoethyl imidazolines, **1** (Fig. 1) have three important structural features: the electron-rich amidine (N=C–N) motif, the hydrophobic alkyl chain R and a short hydrophilic aminoethyl pendant chain. The combination of these structural features is believed to account for the strong film forming behavior of this class of molecules. The N atom at position 3 in the imidazoline ring ($^{3}N=^{2}C-^{1}N$) and the N atom of the amino group in the pendant aminoethyl substituent can be protonated in carbonic acid (i.e. aqueous CO_2,) [1]. This protonation renders alkyl aminoethyl imidazolines amphiphilic such that they behave as cationic surfactants which strongly adsorb on the chloride-rich negatively charged surface of carbon steels immersed in chloride-rich brines. In most cases, effective/optimum coverage of the metal surface is achieved at an inhibitor concentration above the critical micelle concentration (CMC) of the imidazoline surfactant [2]. The industry is demanding corrosion inhibitors which provide efficient inhibition in CO_2 saturated brines at high oilfield temperatures ($T \geq 120°C$). This is a challenging problem for surfactants which rely on an electrostatically driven physi-sorption process to establish a protective film.

The long hydrocarbon tail R is the hydrophobic part of the molecule which promotes aggregation and micellization. An increase in the length of the hydrocarbon chain results in a decrease in the CMC and enhanced aggregation on the metal surface. Zhang et al. [2] reported on

molecular modelling studies on aminoethyl imidazolines with varying length of the saturated hydrophobic chain. The modelling showed a systematic increase in adsorption energy and cohesive energy with increasing chain length, and this was correlated with an increase in inhibitor efficiency, η, as reported by Ramachandran et al. [4]. Yoo et al. [5] found that η depends on hydrocarbon chain length and the degree of unsaturation in the chain. It should be noted that the R group of the commercial imidazoline corrosion inhibitor (Fig. 1) represents a range hydrocarbon chain structures defined by the composition of the TOFA starting material. The main fatty acids in TOFA are linoleic acid and oleic acid. The high degree of unsaturation in tall oil fatty acids is important to optimise the hydrophilic-lipophilic balance and solubility of the imidazoline derivative as compared to analogues based on saturated fatty acids [6].

In general, for a given imidazoline head group structure, we would expect the detailed composition of the fatty acid feedstock to affect surfactant aggregation behavior in terms of hydrophobe-hydrophobe association energies, CMC, aggregation number, packing parameters and micellar structures. These effects would strongly influence the high temperature performance of imidazoline corrosion inhibitors. Another important factor is the stability of the imidazoline head group. At elevated temperatures, particularly in the range 100-150°C, under CO_2 conditions, we might expect significant hydrolysis of the imidazoline ring to form the corresponding amido-amine and other precursors.

A paper by Chen et al. [7] compared the high temperature performance of a tall oil-based aminoethyl imidazoline, **1** and its fatty amido-amine precursor, **2**. The imidazoline, **1** is a free-flowing liquid which is more easily handled and more easily dispersible than its rather waxy amido-amine precursor, **2**. Tests at 149°C indicated inhibition efficiencies in the range of 85-90% after 4, 24 and 72 hours when either the tall oil-based aminoethyl imidazoline or its fatty amido-amine precursor was used at 1000 ppm. This similar high temperature performance is consistent with the likelihood of hydrolysis of the imidazoline back to the amido-amine (although this was not mentioned or concluded in the paper). For both inhibitors, the dosage (1000 ppm) required to achieve reasonable inhibition η=90% at 149°C is 40 times higher than the dosage (25 ppm) required to achieve η=95% at 66°C.

Ramachandran et al. [8] described a water-dispersable high temperature fatty acid/amido-amine corrosion inhibitor which provides protection at 204°C. High dosages (2500-5000 ppm) were used to create thick films which reduced the corrosion rate to 1-2 mpy at 177°C. It was concluded that thicker and more uniform films are more persistent than those given by applying a near-minimum corrosion inhibitor dosage. Subsequently, good film persistency was measured, and film thicknesses (2.7-5.7 μm range) were monitored by optical profiling (white light interferometry). These numbers significantly exceed the film thickness results obtained

using an AFM method for imidazolinium chloride films adsorbed on X65 steel. Xiong et. al. [9] concluded that the structure of the imidazolinium chloride film changes from a monolayer to a bi-layer as the inhibitor concentration exceeds its CMC.

Gough et al. [10] reported on the synthesis, isolation and inhibition performance of imidazoline and amide structures synthesized from oleic acid and diethylenetriamine (DETA). The paper recognizes that commercial ("standard") TOFA/DETA products are mixtures mainly consisting of the aminoethyl imidazoline, the imidazoline amide, the bis-amide and the mono-amide. The performance of each of these components and a mixture of the imidazoline and imidazoline amide was studied in CO_2 saturated seawater at 65°C with 20 vol. % kerosene. The following order of inhibition efficiency η was reported: std. mixture (94-95%) ≈ aminoethyl imidazoline (94-95%) > imidazoline amide (94%) > mono-amide (92.5%) > bis-amide (61%). Interestingly, in "bubble" tests wherein the inhibitor is injected into the oil phase, the η order was std. mixture (95%) < aminoethyl imidazoline (97%) < mono-amide (99%); and the imidazoline amide and bis-amide had no inhibition efficiency as they remained in the oil phase. In a further paper [11], Gough et al. describe molecular modelling studies on some of the imidazolines and amides described in the first paper [10].

A thorough literature review demonstrated that corrosion inhibitors and their products of hydrolysis are generally performance tested with a focus on the uniform corrosion behavior. The present study emphasises the effects of inhibitor hydrolysis on both uniform and localized corrosion. This paper focuses on an evaluation of the molecular characteristics of a TOFA/DETA based imidazoline inhibitor, including (i) analysis of the inhibitor protonation profile in aqueous acid, determination of CMC and the micelle size in salt-free water and CO_2 saturated 3 wt. % NaCl at elevated temperature, (ii) investigation of hydrolysis of the imidazoline inhibitor at various temperature and pH conditions and (iii) analysis of uniform/localized corrosion behavior of X65 carbon steel at 80°C in the presence of fresh and pre-aged imidazoline inhibitor in brines consisting of 3 wt. % NaCl saturated with CO_2.

2.0 Experimental Procedure

2.1 Brine preparation and corrosion inhibitor

A 3 wt. % NaCl brine, prepared by dissolving analytical grade NaCl (Sigma-Aldrich) in distilled water was used. Brine consisting of 3 wt. % sodium chloride (NaCl) in distilled water was prepared by CO_2 bubbling of the brine for a minimum of 2 h prior to an experiment. The brine was then also bubbled with CO_2 during each experiment. The corrosion inhibitor was always injected into the brine before the experiment had commenced using a 10-100 µL pipette. The inhibitor used for these experiments is an imidazoline based corrosion inhibitor which was

synthesized by reacting tall oil fatty acid (TOFA) with diethylene triamine (DETA). The inhibitor is a light-yellow viscous liquid. The inhibitor was supplied by M-I SWACO.

2.2 Conductivity and pH titration measurements

Conductivity measurements of aqueous inhibitor solutions (in deionised water) were conducted at 20±0.1°C using a Mettler-pH/Ion/Cond meter SGD Pro SG78-ELK. The calibration was performed with a 500 µs cm^{-1} standard solution. At each inhibitor concentration, the conductivity was monitored every 5 min until steady state was reached. To determine the critical micelle concentration (CMC) of the corrosion inhibitor, the solution conductivity was measured at concentrations ranging from 0 to 30 ppm. The resulting conductivity curves were plotted as two linear regression segments having different slopes in the pre-micellar and post-micellar regions and the CMC value was determined from the breakpoint. Each measurement was repeated twice.

For the potentiometric studies, the inhibitor (0.5 g) was dispersed in 0.5 L of 3 wt. % NaCl brine at 70°C and was then subsequently titrated with 0.1 M HCl prepared using 3 wt. % NaCl. Each titration point was recorded until the potential drift was stable. Each measurement was repeated twice. The equivalence points were determined by using the conventional method of taking the first derivative of the pH with respect to volume of acid added, with the minima of this representing the equivalence points.

2.3 Dynamic Light Scattering (DLS)

A Malvern Zetasizer Nano ZS was used to characterize micellar sizes of the imidazoline based corrosion inhibitor. The analysis was done in two testing solutions: (i) deionized (DI) water at 20.0±0.1°C and (ii) CO_2 saturated 3 % NaCl brine at 70±0.1°C. The inhibitor was introduced to the system stepwise and mixed thoroughly on a stirrer plate throughout the experiment. After each inhibitor addition, the solution was left to mix for 0.5 h. For DLS analysis, 1 mL sample was collected from the stock solution, filtered with a 0.2 µm filter of mixed cellulose acetate to remove any interfering dust particles and transferred into a disposable polystyrene cuvette making sure no bubbles were present. The temperature 20±0.2°C or 70±0.2°C of the solution was maintained throughout the DLS measurement. Each sample was scanned between 7 to 12 times. The volume mean micelle diameter D_h and the count rate were recorded as average values over all scans.

2.4 Spectroscopic analysis

^1H NMR spectra were recorded on a Bruker 400 MHz spectrometer in $CDCl_3$ solution. Fourier transform infrared (FTIR) spectra were recorded using a Nicolet iS50 FTIR spectrometer which was equipped with an attenuated total reflection (ATR) accessory.

2.5 Determination of hydrolysis constant of the corrosion inhibitor by ATR FTIR spectroscopy

The hydrolysis of the micellar solutions of corrosion inhibitor were carried out in a 0.3 L bench top PTFE-lined PARR autoclave made of Hastelloy and equipped with gas inlet/outlet valves, and a liquid sampling valve. 0.2 L of 3% NaCl brine solution and 20 mg of the corrosion inhibitor was added to the autoclave, and a constant CO_2 flow was purged in the solution for 0.5 h to remove residual dissolved oxygen. The autoclave was assembled and then pressurized with CO_2 gas to a total pressure of 2 bar at 25°C. The experiment was conducted at 70, 85, 100 and 120°C for 8 h at a stirrer speed of 500 rpm. For the 100 and 120°C experiments, the autoclave was additionally pressured with pure Argon gas to a total pressure of 150 psi to avoid water evaporation. When the autoclave is heated to the desired temperature, fluid aliquots are continuously collected during the experiment before purification and analysis by ATR FTIR.

The following procedure was used to analyse the composition of the degraded corrosion inhibitor: transfer a 15-20 ml aliquot of the degraded micellar solution to a 250 ml separating funnel, add 100 ml of dichloromethane (DCM) and 50 ml of DI water, vigorously shake for 5 min, and leave for 0.5-1h for phase separation. After separation is complete, transfer the DCM bottom layer to another separation funnel and repeat the washing of the sample solution with DI water at least 5 times. Transfer the DCM layer to a flask, add 3-5 g of anhydrous sodium sulphate desiccant, mix and remove the sodium sulphate by filtration. Evaporate the DCM extract at reduced pressure at 50-70°C. Use a Pasteur glass pipette to transfer the residue (aged inhibitor) onto the diamond window of the Nicolet iS50 ATR FTIR spectrometer for compositional analysis. The intensity of the imidazoline and amide absorption bands at 1607 cm^{-1} and 1646 cm^{-1}, respectively, were measured.

The apparent first-order rate constant, k_{app} of the hydrolysis of the imidazoline inhibitor in a 3 wt. % NaCl brine saturated with CO_2 was determined from linear plots based on the following equation:

$$\ln\left(\frac{Abs_{1607}}{Abs_{1646}}\right) = -k_{app}\ t_{1/2} \qquad (1)$$

where $t_{1/2}$ is the half-time of the reaction, $\frac{Abs_{1607}}{Abs_{1646}}$ is the time-dependent spectral ratio of the imidazoline and amide components of the aged inhibitor. The apparent rate constants were obtained by linear regression with coefficient $r \sim 0.99$.

2.6 Specimen preparation

X65 carbon steel samples were machined to have dimensions of 2.5 cm diameter and 0.6 cm thickness. A single Kapton insulated wire was soldered to each X65 carbon steel specimen. The

specimen was then embedded within a resin. Each X65 steel coupon had an exposed steel surface area of 4.9 cm^2. The specimens were further prepared prior to each corrosion test by wet-grinding up to 600 silicon carbide (SiC) grit. X65 steel coupons were then rinsed using acetone and distilled water. Two carbon steel coupons were used for each corrosion test in 1L sodium chloride brines. The carbon steel used in these tests has a ferritic-pearlitic microstructure with the following composition (Table 1).

Table 1: X65 carbon steel elemental composition (wt. %)

C	**Si**	**Mn**	**P**	**S**	**Cr**	**Mo**	**Ni**
0.12	0.18	1.27	0.008	0.002	0.11	0.17	0.07
Cu	**Sn**	**Al**	**B**	**Nb**	**Ti**	**V**	**Fe**
0.12	0.008	0.022	0.0005	0.054	0.001	0.057	Balance

2.7 Electrochemical LPR measurements

Linear polarization resistance (LPR) was utilized to monitor the corrosion response and to assess the generalized corrosion inhibitor performance. The polarization resistance, corrosion rate and open circuit potential (OCP) were monitored and recorded with time. The corrosion rates were calculated based on a Stern-Gear coefficient (B) of 14.4 mV obtained for fresh inhibitor (30 ppm) at steady state (24 h). The three-electrode cell configuration consisted of a combined silver/silver chloride (Ag/AgCl) reference/counter electrode and a X65 steel coupon (working electrode). The working electrode was polarised using an ACM Gill 8 potentiostat at ±15mV with respect to the open circuit potential at 0.25 mV/s. Linear polarization measurements were recorded every 15 min.

2.8 pH measurements during corrosion tests

A Thermo Scientific Orion Star A211 benchtop meter integrated with automatic temperature correction was used to measure the brine pH. The pH meter was calibrated prior to each experiment. The measurement probe was equilibrated in the brine for approximately 3 min prior to each recording.

2.9 Inhibitor aging at 80°C

For inhibitor aging experiments, 30 ppm inhibitor was injected into 1L of CO_2 saturated 3 wt. % NaCl brine using a glass cell setup, which was then heated to 80°C for 24, 48 or 120 h. Once the inhibitor had been aged for the desired duration, specimens were inserted into the brine

containing the aged inhibitor and electrochemical measurements were recorded for 48 h at 80°C. The stir rate and extent of CO_2 sparging were kept constant.

2.10 Inhibitor aging at 120°C

Pre-aging of the inhibitor at 120°C was performed using an autoclave setup as shown in our paper [12]. The brine solution was first prepared and equilibrated with CO_2 for 24 h in the glass cell configuration at room temperature. The corrosion inhibitor was then injected into the brine contained within a 1L glass vessel. After 30 minutes, the brine solution containing the inhibitor was pumped into the autoclave through flowlines which had been flushed out with CO_2 in order to avoid oxygen contamination. The autoclave was sealed at atmospheric pressure before being heated to 120°C. The inhibitor was aged in the brine solution for 2, 6 or 24 h at 120°C before being cooled to 80°C and transferred back into a new glass vessel and allowed to reach a stable temperature of 80°C before insertion of the carbon steel test specimens. The pre-aged inhibitor was then performance-tested at 80°C for 48 h with continuous CO_2 bubbling and magnetic stirring (100 rpm).

2.11 Surface analysis methods

2.11.1 Scanning electron microscopy (SEM)

A Carl Zeiss EVO MA15 VP SEM was used to record images of the carbon steel coupons from a top-view perspective. The carbon steel coupons were prepared by removing the specimens from their resins and coating their outer edges with carbon. The images were acquired at 5-30 kV and 0.1-5 nA.

2.11.2 NP_{FLEX} 3D surface metrology

A Bruker 3D surface profiler was used for post-test analysis to determine and examine the extent of localized corrosion on X65 coupons. The X65 coupons were first cleaned of any corrosion products exiting on the steel surface. This was conducted using Clarke's solution in accordance with ASTM Standard G1-03. For each experiment, four 9 mm^2 areas were profiled across 2 coupons. The ten deepest pits recorded across all 4 regions were then averaged to represent the pit depth. The profiler was used at an objective of 2.5X and 3.5 mm working distance.

3.0 Results and discussion

3.1. Composition and molecular characteristics of imidazoline based corrosion inhibitor

The general structure of the imidazoline based inhibitor is given in Fig. 1. The inhibitor is manufactured in a two-stage process involving a double condensation reaction of diethylenetriamine (DETA) and tall oil fatty acid (TOFA) [13-15]. Commercially available TOFA,

Sylfat^{R} 2R (Kraton Polymers LLC) was used for the industrial synthesis of the corrosion inhibitor used in the present study. Sylfat^{R} 2R has a high fatty acid content and low content of rosin acids and unsaponifiables. The unsaturated fatty acids in TOFA tend to lower the melting point of the DETA/TOFA-based inhibitor such that it is a liquid product at room temperature.

In general terms, the DETA/TOFA based inhibitor is a complex mixture containing multiple molecular structures including the imidazoline **1**, the amido-amine precursor **2**, the diamide and the imidazoline amide, etc. [10,11,13,16,17]. ^{1}H and ^{13}C NMR and FTIR spectroscopy (Fig. 1 in ESI†) was used to characterize the composition of the corrosion inhibitor mixture. The main components are the aminoethyl imidazoline **1** and its precursor, the amido-amine **2**. Analysis of the ratio of protons in the terminal methyl-CH_3 group to other characteristic protons of the inhibitor (e.g. δ=3.7 ppm for C(2)H_2 in structure **1,** [Fig. 1 in ESI†]) suggest that the relative concentration of imidazoline **1** in the mixture is 55 %. The ^{13}C NMR spectrum shows signals associated with three different amides at δ 173.33, 173.42 (main signal) and 173.66 ppm and two different imidazoline signals assigned to the C=N bond within the imidazoline ring at δ 168.01 (main signal) and 167.57 ppm, consistent with at least two components. The FTIR spectra show characteristic adsorption bands of imidazoline **1** and the amide of amido-amine **2** structure: 1655 cm^{-1} (C=O, Amide I), 1554 cm^{-1} (N-H stretch, Amide II) and 1608 cm^{-1} (C=N- and C-N stretch).

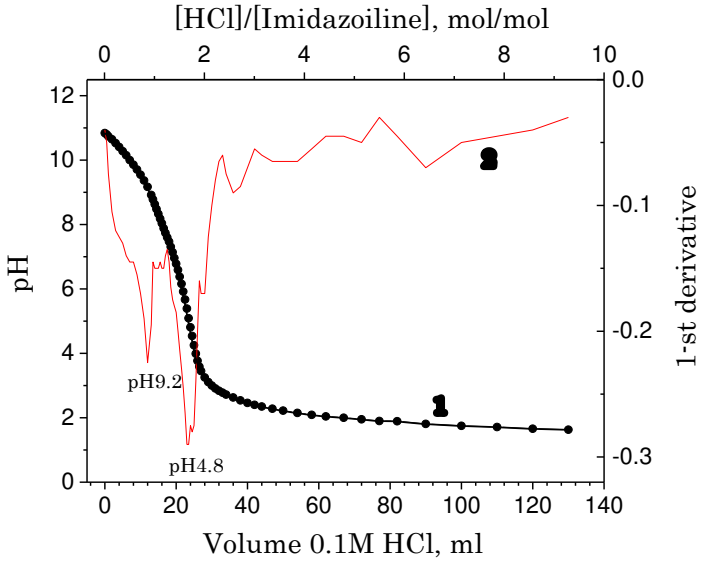

Figure 2: The titration curve (1) and the first pH derivative (2) for 1000 ppm solution of corrosion inhibitor in 3 wt. % NaCl brine titrated with 0.1 M HCl prepared in 3 wt. % NaCl. The initial pH of the corrosion inhibitor solution was 10.4.

Due to variable pH conditions under different downhole environments, it is important to establish a protonation profile of the inhibitor to better understand its chemistry and the

species responsible for its corrosion inhibition performance. Potentiometric titration (Fig. 2) was used to determine the equivalency point (EP) of the inhibitor in 3% NaCl brine with the assumption that hydrolysis of imidazoline **1** does not occur under testing conditions. Two equivalency points at pH 9.2 and pH 4.8 were observed. Based on analysis of literature data [18,19], modelling using Chemicalize [20] and considering that the DETA/TOFA-based corrosion inhibitor is a mixture of imidazoline **1** and amido-amine **2**, we can assume the following protonation sequence of the inhibitor mixture as shown in Fig. 4. The pH value of pH 9.2 represents equivalency points for protonation of the C=N (imine) group to form imidazoline **1'** and of the primary amine (-NH_2) to form amide **2'**. The second equivalency point at pH 4.8 represents protonation of the primary amine (-NH_2) of the aminoethyl pendant group to form imidazoline **1''** and of the secondary amine >NH group to form amido-amine **2''**, correspondingly.

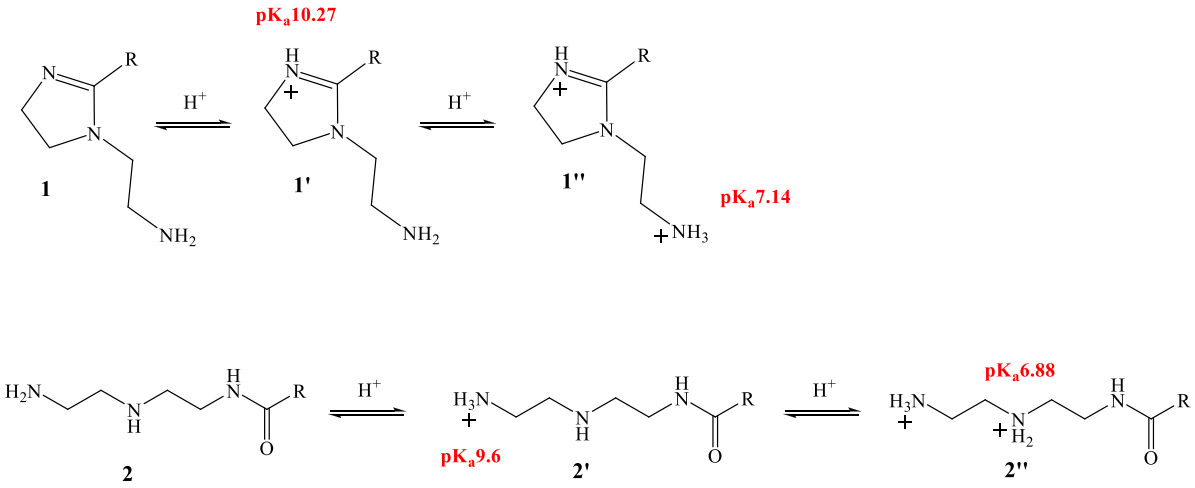

Figure 3: pK_a values and the sequence of protonation of N atoms of imidazoline **1** and amido-amine **2** calculated using Chemicalize for R=C_3H_7.

Protonation of the imidazoline plays a two-fold role in the performance of the corrosion inhibitor: the protonation (i) increases solubility/dispersibility of the inhibitor in CO_2 saturated 3 wt. % NaCl brine at pH~4.1 and (ii) enhances molecular adsorption of the positively charged imidazoline on the metal surface, thereby improving inhibition performance. The potentiometric titration data also suggests that at pH 4.1 the two-step protonation of the imidazoline is completed. It should be noted that increasing the pH of the solution during the corrosion experiment will also affect the degree of protonation of the inhibitor.

In their protonated state, imidazolines belong to the category of cationic surfactants which are highly dispersible in brine solutions and above a critical concentration spontaneously form ordered structures (micelles) [21]. It has been established that there is a relationship between the CMC, the formation of an adsorbed surfactant monolayer/bilayer on the metal surface and

the corrosion inhibition performance of imidazoline based inhibitors. Temperature, salt concentration and pH may have a profound effect on the CMC and on the aggregation number of the micelles in aqueous media [22]. In the present work, a conductivity study and DLS measurements was used to determine the CMC and the micelle size of the inhibitor in DI water and in CO_2 saturated 3 wt. % NaCl brine at 20 and 70°C.

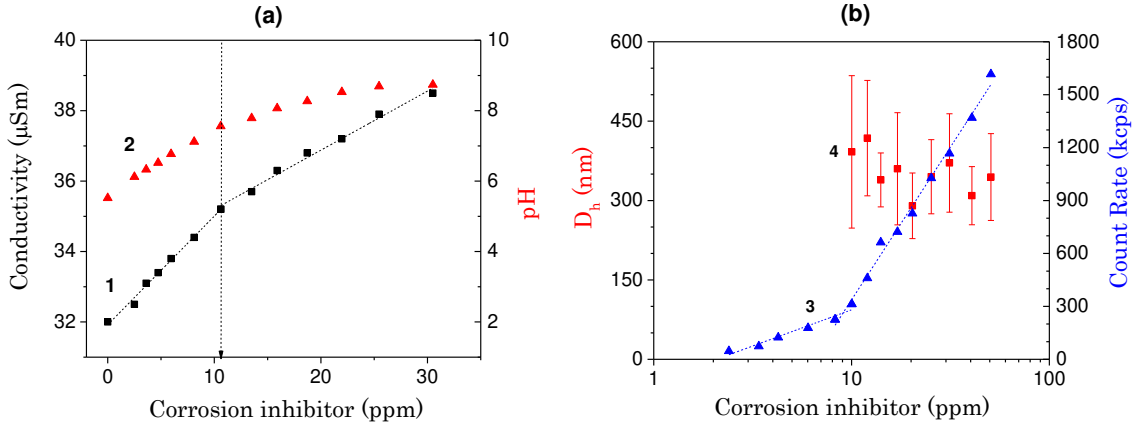

Figure 4: Conductivity (1), pH (2), mean hydrodynamic diameter, D_h of micellar solution (3) and count rate (4) as a function of inhibitor concentration in DI water at 20°C.

The CMC value was determined from the change of slope in conductivity values versus inhibitor concentration as shown in Fig. 4. The DLS data (Fig. 4, b) shows that at inhibitor concentrations above the CMC, the intensity of light scattering (count rate) increases significantly and the autocorrelation function yields a robust value for the hydrodynamic diameter of micelles. The onset of the D_h plateau also roughly indicates the CMC of the imidazoline inhibitor. Both methods indicate that the CMC of the imidazoline inhibitor is 12±2 ppm in DI water at 20°C. The average hydrodynamic diameter of the imidazoline micelles is 329±70 nm and the hydrodynamic diameter distribution is polydisperse. In the present experiment (Fig. 4), the pH of the solution increases markedly with increasing concentration of the inhibitor and, therefore, the degree of protonation of the inhibitor decreases, which could affect the CMC value. The pH of the inhibitor solution at the CMC (12 ppm) is 7.56 which means that the imidazoline ring is fully protonated (**1'** in Fig. 3) and primary N atom is only partially protonated (**1''** in Fig. 3).

Fig. 5 shows the micelle size of the imidazoline dispersion represented by the volume mean hydrodynamic diameter and the count rate in CO_2 saturated 3 wt. % NaCl brine at 70°C. Acetic acid solution was added to maintain a constant pH=4.1 for all inhibitor concentrations. For comparison, in a control experiment (Fig. 6, curve 2), acetic acid was not added such that the pH increased with inhibitor concentration leading to progressive change in the degree of protonation of the inhibitor. In both the pH 4.1 and pH 4.1→5.6 experiments, the CMC was 10±1 ppm (~29 μM). The CMC value for the imidazoline based inhibitor used in the current work is in

agreement with that reported by Mazumder et al. [2], Nesic et al. [23], and Ali et. al. [24]. In contrast, when present in a strongly acid environment, it has been reported that an imidazoline surfactant derived from DETA/Oleic acid has a much higher CMC value of 0.18 mM (~63 ppm) and 0.22 mM (~77 ppm) for 1M HCl and 1M H_2SO_4 solutions, respectively [19].

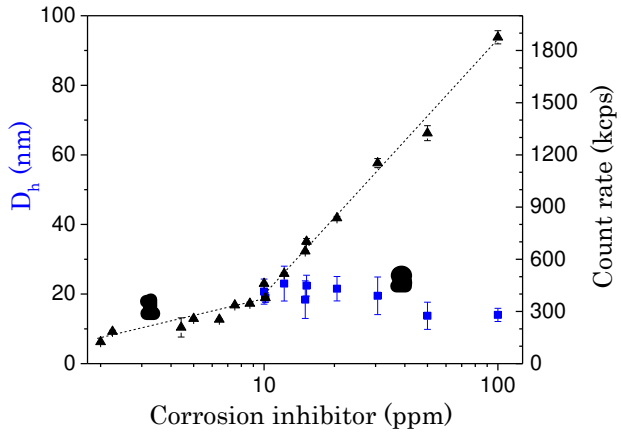

Figure 5: A plot of the intensity of light scattering (1) and the mean hydrodynamic diameter (2) obtained for various concentrations of the corrosion inhibitor prepared in CO_2 saturated 3 wt. % NaCl brine at 70°C. Acetic acid, 0.05M, was added to the 3 wt. % NaCl brine to maintain pH 4.1 during these measurements. The intersection of the two lines at 10±1 ppm in the count rate data corresponds to the CMC.

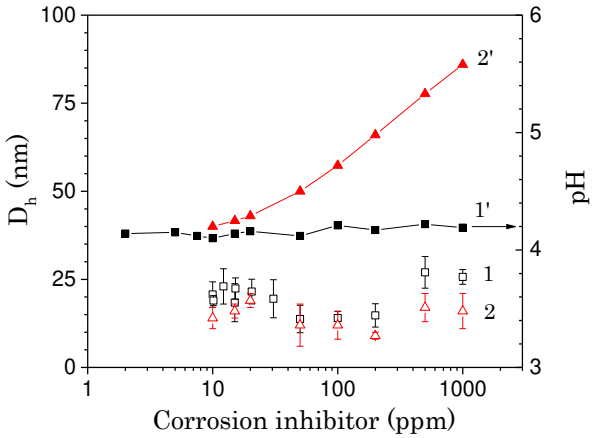

Figure 6: Variation of the mean hydrodynamic diameter, D_h (1, 2) and pH (1',2') as a function of the corrosion inhibitor concentration in CO_2 saturated 3 wt. % NaCl brine at 70°C. 1, 1' – pH value (4.1 – 4.2) is maintained using acetic acid (0.05M solution in 3 wt. % NaCl). 2, 2' – pH value is not maintained.

As can be seen in Fig. 6, the characteristic micelle size in a CO_2 saturated 3 wt. % NaCl brine at CMC concentration is 18±9 nm. It is also clearly seen that a change in the concentration of the

inhibitor in the range from 10 to 1000 ppm (from 1 to 100 CMC) and the pH of the solution (curves 2 and 2' in Fig. 6) does not seriously affect the micelle size.

The last important point that we want to pay attention to is the low solubility of the amido-amine based precursor **2** in a saturated CO_2 3 wt. % NaCl brine. In this regard, we believe that an important role played by the imidazoline **1** is to co-solubilize the less soluble amido-amine based precursor **2** by mixed micellisation and to then deliver the amido-amine **2** with the imidazoline **1** to the metal surface. This mechanism becomes critical for thermally degraded imidazoline based inhibitors wherein the residual concentration of imidazoline **1** has decreased and the concentration of the amido-amine **2** has increased.

3.2 Degradation of DETA/TOFA based inhibitor by acid catalyzed hydrolysis

Hydrolysis of imidazoline **1** is known as a two-step reaction (Fig. 7) and hydrolysis occurs in both basic and acidic media [25]. Harnsberger and Riebsomer [26] reported that the hydrolysis reaction rates for 1,2-dialkyl-2-imidazolines are strongly influenced by various ring substituents and the hydrolysis is catalysed by bases and inhibited by acids. The introduction of a branched substituent into the imidazoline ring increases the hydrolytic stability of the compounds [27]. There is no well-established view in the literature about the effect of protonation of the N atom at position 3 in the imidazoline ring ($^{3}N=^{2}C-^{1}N$) at pH<7 on the stability of the imidazoline and, more generally, detailed relationships between inhibitor composition and resistance to hydrolysis [13,19,25,27]. Bondareva et al. [27] showed that hydrolysis occurred under alkaline conditions but at pH<6 hydrolysis was not observed, apparently due to protonation at the N atom at position 3 in the imidazoline ring. However, there is agreement that the rate of hydrolysis is dependent on pH and temperature [28]. Moreover, Martin and Valone [13] emphasized that the imidazoline **1** in imidazoline formulated corrosion inhibitors is spontaneously and rapidly converted into the amido-amine precursor **2**, and that there is no significant difference in the corrosion protection given by inhibitors formulated with imidazoline **1** or its precursor amido-amine **2**.

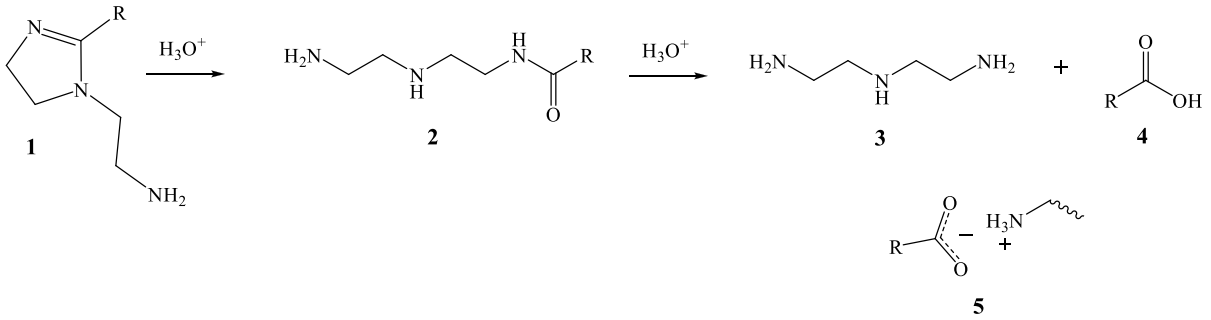

Figure 7: Two step hydrolysis of imidazoline: (Step 1) ring-opening from imidazoline **1** to amido-amine **2** and (Step 2) cleavage of amide group yielding DETA **3** and TOFA **4**. The primary and secondary amine groups of **1**, **2** and **3** can be protonated by TOFA **4** to form organic salts **5**.

Thus, hydrolysis of the imidazoline based inhibitor in CO_2 saturated brine proceeds via the first step mechanism (Fig. 7) resulting in a decrease in the concentration of imidazoline **1** and an increase in the concentration of amido-amine **2**. Accordingly, during aging of the inhibitor solution, we would expect a decrease in the ratio of the concentration of imidazoline **1** to the concentration of amido-amine **2.** Further second step hydrolysis of the amido-amine **2** to form the acid (TOFA) and the amine (DETA) will also affect the imidazoline/amido-amine ratio. Complete hydrolysis of the inhibitor will result in the disappearance of imidazoline **1** and amido-amine **2** and the formation of precursors **3** and **4** (the original reactants used to synthesise the inhibitor) as shown in Fig. 7.

As described in the experimental section, for ATR FTIR analysis, sub-samples taken during the hydrolysis of the inhibitor solution (in an autoclave at an elevated temperature) were extracted with pure DCM in order to quantitatively transfer the corrosion inhibitor and its hydrolysis products from the aqueous phase to the organic phase. The DCM extraction method was validated by analysis of the imidazoline **1** to amido-amine **2** ratio in fresh (not aged) solutions of the corrosion inhibitor and in model blends. The ratio of absorption bands at 1607 cm^{-1} and 1646 cm^{-1} for the fresh corrosion inhibitor and treated with the brine-DCM extraction method remained unchanged. This also means that imidazoline **1** and amido-amine **2** species are equally partitioned into DCM phase during extraction from its aqueous dispersion.

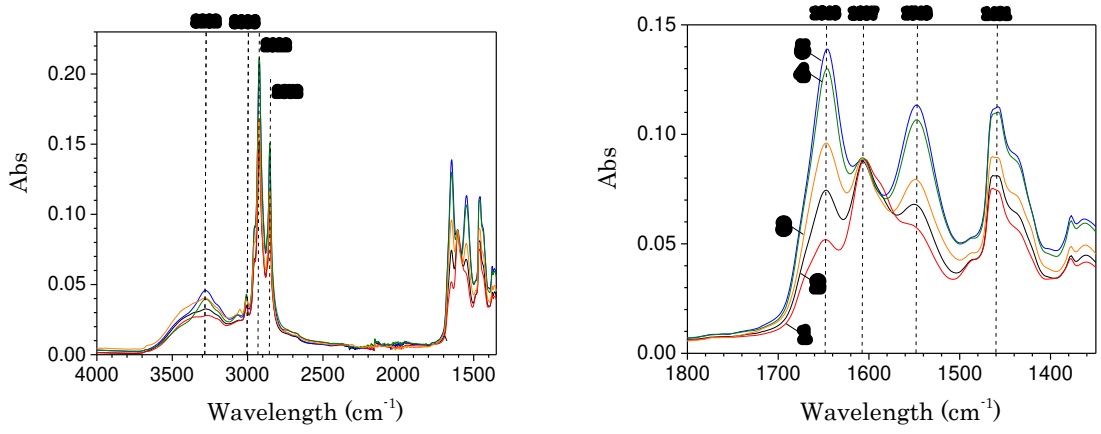

Figure 8: ATR FTIR spectra of the imidazoline based corrosion inhibitor and its hydrolysis products after aging in 2 bar CO_2 saturated 3 wt. % NaCl brine at 100°C for 0.4 h (1), 1.2 h (2), 3 h (3), 5 h (4), 7 h (5). The spectra have been normalized with respect to the absorbance of the band at 1607 cm^{-1}.

The ATR FTIR spectra (Fig. 8) of the imidazoline based corrosion inhibitor and its hydrolysis products formed in CO_2 saturated 3 wt. % NaCl brine at 100°C show considerable overlap between the bands due to imidazoline **1** and amido-amine **2**. The broad band peaking at 3282 cm^{-1} (N-H stretch) is due to bond vibrations in **1** and **2**; the band at 3006 cm^{-1} (-CH=CH-: C-H stretch) is also due to bond vibrations in **1** and **2**; and the bands at 2922 and 2852 cm^{-1} (>CH_2: C-H stretch) are due to contributions by structures **1** and **2**. The absorbance band at 1646 cm^{-1} (C=O, stretch) is due to the amido-amine **2**. The band at 1607 cm^{-1} (C=N, stretch) is characteristic of structure **1**. The broad band at 1548 cm^{-1} is characteristic of structure **1** (N-H, C-N) and salt **5** ν(C=O stretch). The band at 1461 cm^{-1} (>CH_2: C-H scissor) is due to both structures **1** and **2**. As seen in Fig. 8, during aging of the inhibitor, the absorbance of the band at 1646 cm^{-1} (due to amido-amine **2)** increases with aging time, indicating progressive hydrolysis of the imidazoline **1**.

The ATR FTIR analysis method did not detect the presence of DETA **3** and TOFA **4** in the extracts of the inhibitor solutions aged at elevated temperature (70 – 120°C). The ATR FTIR spectrum of pure TOFA **4** reveals a strong characteristic absorbance band at 1710 cm^{-1} but this is not seen in the extracts of the aged inhibitor solutions due to deprotonation by primary and secondary amines, as shown in Fig. 7. However, the appearance of a carboxylate band at 1548 cm^{-1} in the extracts (Fig. 8) indicates the formation of salt **5** by reaction of TOFA **4** with the primary amino group in the amido-amine **2** and/or the primary amino group of the aminoethyl pendant group of the imidazoline **1**.

Thus, in the present study, the ratio of the absorbance of the characteristic bands due to imidazoline **1** and amido-amine **2**, Abs 1607 cm^{-1}/ Abs 1646 cm^{-1}, was used to monitor the *relative* quantities of imidazoline **1** and amido-amine **2** in DCM extracts of the fresh and aged inhibitor solutions. For reasons mentioned previously, the DCM extraction method cannot be used to monitor the products of the second step reaction.

We investigated two key factors which control the rate of inhibitor hydrolysis: solution pH and temperature. The effect of the initial pH on the rate of hydrolysis, as determined by the ratio Abs 1607 cm^{-1}/ Abs 1646 cm^{-1}, in CO_2 saturated 3 wt. % NaCl brine is illustrated in Fig. 9. The initial pH conditions were pH=4.1 (1) and pH=6.0 (2). The higher initial pH condition was achieved by the addition of a solution of sodium bicarbonate $NaHCO_3$ (0.1M in 3 wt. % NaCl). Pseudo first-order kinetics were observed, and half-lives of the reaction were determined graphically (Eq. 1). The half-lives of the inhibitor aged at 70°C are $t_{1/2}$ =25.1 h for initial pH=4.1 and $t_{1/2}$=7.4 h for initial pH=6.0.

The effect of temperature was studied for solutions containing 100 ppm inhibitor concentration aged in 3 wt. % NaCl brine at 2 bar CO_2 in the autoclave (Fig. 10, a). For a given temperature, a linear relationship between the natural logarithm of the ratio Abs. 1607 cm^{-1}/Abs. 1646 cm^{-1} and aging time was observed (Fig. 10, b). It should be noted that the rate of inhibitor hydrolysis slightly increases when the CO_2 partial pressure is increased: compare $t_{1/2}$ = 25.10 h at atmospheric CO_2 pressure with $t_{1/2}$ = 20.49 h at 2 bar CO_2, each determined at 70°C and initial pH 4.1.

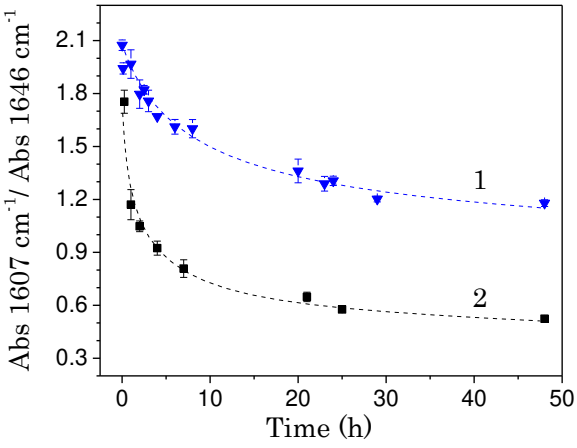

Figure 9: Effect of pH on evolution of ATR FTIR ratio Abs. 1607 cm^{-1}/Abs. 1646 cm^{-1} for 100 ppm inhibitor solution aged in CO_2 saturated 3 wt. % NaCl brine, 70°C. The initial pH conditions were pH=4.1 (1) and pH=6.0 (2).

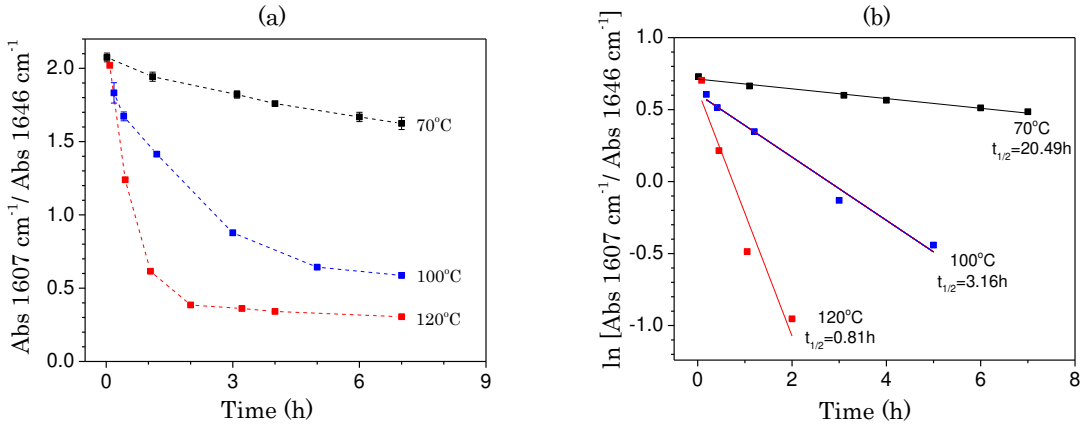

Figure 10: Pseudo-first-order plots for hydrolysis of imidazoline **1** to amido-amine **2** based on ATR FTIR adsorption ratio (Abs. 1607 cm^{-1}/Abs. 1646 cm^{-1}) for 100 ppm inhibitor solution aged in 2 bar CO_2 saturated 3 wt. % NaCl brine at 70, 100 and 120°C, initial pH 4.1.

The effect of temperature on the degradation rate of the inhibitor is shown in Fig. 11. The activation parameters for hydrolysis of the imidazoline based inhibitor were determined from the temperature dependence of the half-life of the reaction, $t_{1/2}$:

$$t_{1/2} = A \exp\left(\frac{E_a}{RT}\right) \qquad (2)$$

where A is the pre-exponential factor, E_a is the activation energy of the reaction, R is the universal gas constant [8.314 J (mol K)$^{-1}$] and T is temperature (K).

The activation energy of the inhibitor hydrolysis reaction in 2 bar CO_2 3 wt. % NaCl brine is 17.2±0.7 kcal mol^{-1} (72.0±2.9 kJ mol^{-1}). This result is similar to data published for similar imidazoline molecules. For example, 16.5 kcal mol^{-1} (69.2 kJ mol^{-1}) for an imidazoline with fully saturated chain R=$C_{10}H_{21}$ in NaOH solution at pH~12 [29] and 44.6–54.6 kJ mol^{-1} for substituted 1-hydroxyethyl-2-alkyl imidazolines at pH~12 [27] determined by UV spectroscopy from the intense absorption π→π* band at 230-235 nm, which corresponded to the transition of the C=N bond in the heterocycle.

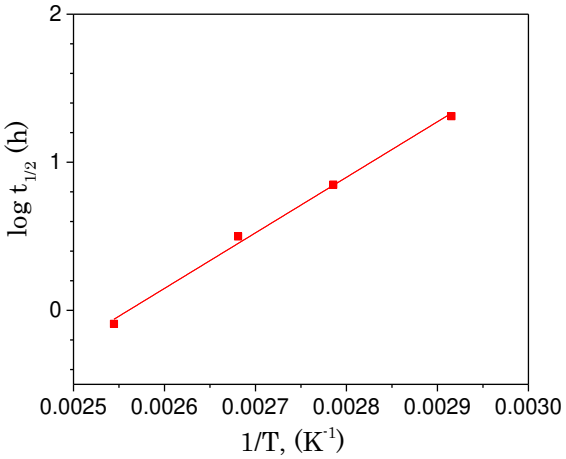

Figure 11: Temperature dependence of the half-life of the hydrolysis reaction $t_{1/2}$ during aging of imidazoline based corrosion inhibitor in 2 bar CO_2 saturated 3 wt. % NaCl brine.

3.3 The corrosion performance of fresh and aged inhibitor

The corrosion performance of the imidazoline based corrosion inhibitor was studied for wet-ground X65 carbon steel exposed to 3 wt. % NaCl brine saturated with CO_2 at 80°C. All electrochemical experiments were performed at an inhibitor concentration of 30 ppm. As shown in our previous publication [12], 30 ppm is the optimal dosage of inhibitor in terms of generalized corrosion. Pre-aging (degradation) of the inhibitor was carried out in CO_2 saturated 3 wt. % NaCl brine at 80°C for 24–120 h, and at 120°C for 2–24 h. After completing the aging procedure, the aged inhibitor solution is transferred back to a glass vessel, where it is allowed to

reach a stable temperature of 80°C before a carbon steel specimen is introduced, and then the effectiveness of the corrosion inhibitor was studied using electrochemical measurements.

3.3.1 Aging at 80°C

Fig. 12 and Table 2 show the corrosion performance for fresh and aged inhibitor at 80°C. The results indicate that $1/R_p$ decreased at a greater rate and reached a lower value when the inhibitor had been aged for 24 to 48 h at 80°C. This suggests that the imidazoline had been at least partially converted into degradation product(s) resulting in improved inhibitor performance. This is consistent with the findings of Jenkins [30] who observed similar behavior after aging for 24 h at a temperature of 100°C. In accordance with our ATR FTIR analysis, it appears that an increase the relative concentration of the amido-amine **2** significantly improves inhibition performance. However, more prolonged pre-aging of the imidazoline inhibitor (120 h at 80°C) led to a reduction in inhibition performance, as seen by a greater value of $1/R_p$ at the end of the 48 h experiment.

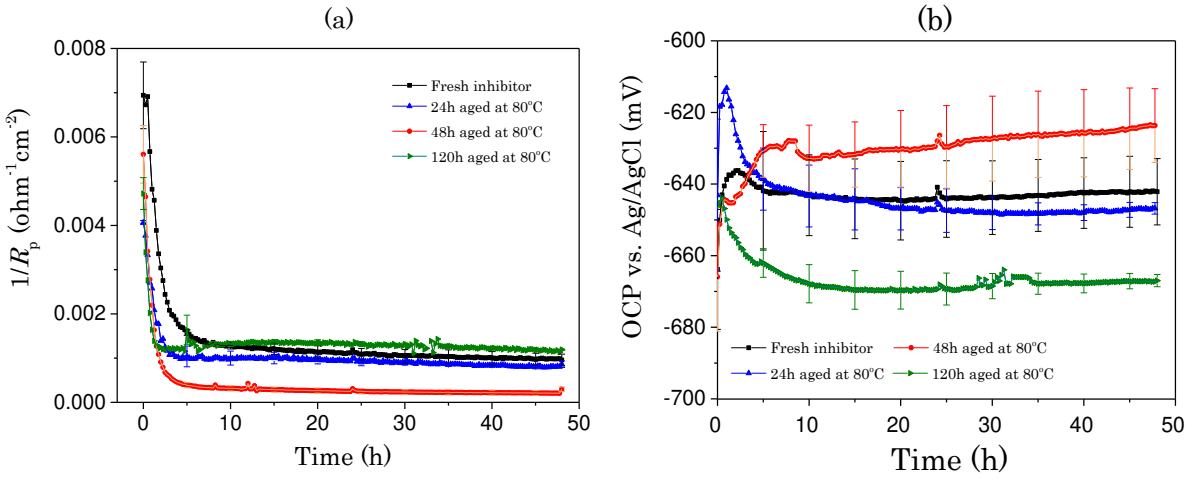

Figure 12: Reciprocal of polarization resistance (a) and OCP (b) versus exposure time for X65 at 80°C in CO_2 saturated 3 wt. % NaCl brine with 30 ppm imidazoline based corrosion inhibitor pre-aged for 0, 24, 48 and 120 h at 80°C.

Table 2: Corrosion rate versus exposure time for X65 at 80˚C in CO_2 saturated 3 wt. % NaCl brine with 30 ppm imidazoline based corrosion inhibitor pre-aged for 0, 24, 48 and 120 h at 80°C.

	Corrosion rate (mm/year)			
Time (h)	**Fresh inhibitor**	**Aged 24 h**	**Aged 48 h**	**Aged 120 h**
0	1.15	0.67	0.93	0.78
1	0.80	0.42	0.36	0.27
2	0.50	0.23	0.15	0.20
5	0.26	0.17	0.06	0.27
10	0.21	0.16	0.05	0.21
24	0.19	0.16	0.05	0.21
48	0.15	0.14	0.05	0.19

The pH of the solution was also measured throughout corrosion testing, since as previously established [12], pH increases with the extent of corrosion and so is indicative of how much corrosion has taken place. Fig. 13 shows the brine pH measured in the corrosion vessel as a function of time. pH measurements revealed that the end-point pH was reduced from pH 4.33 for the fresh inhibitor to pH 4.28 and pH 4.07 for the inhibitor aged for 24 and 48 h, respectively. This is consistent with electrochemistry data and shows that metal dissolution is slower in the presence of the aged inhibitor relative to the fresh inhibitor. When the inhibitor was pre-aged for 120 h, the end-point pH was 4.58, consistent with a decrease in inhibition efficiency with pre-aging time. Thus, the end-point pH values are useful for ranking overall corrosion rates and they confirm the conclusions drawn from electrochemical measurements.

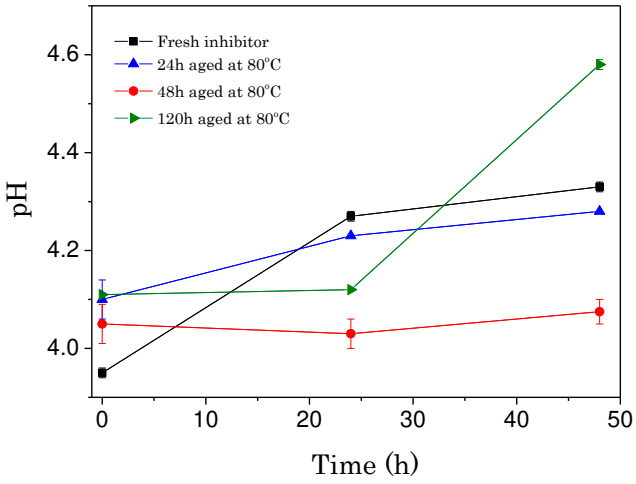

Figure 13: Brine pH at 80°C for X65 in 3 wt. % NaCl brine saturated with CO_2 with 30 ppm imidazoline based corrosion inhibitor pre-aged for 0, 24, 48 and 120 h at 80°C.

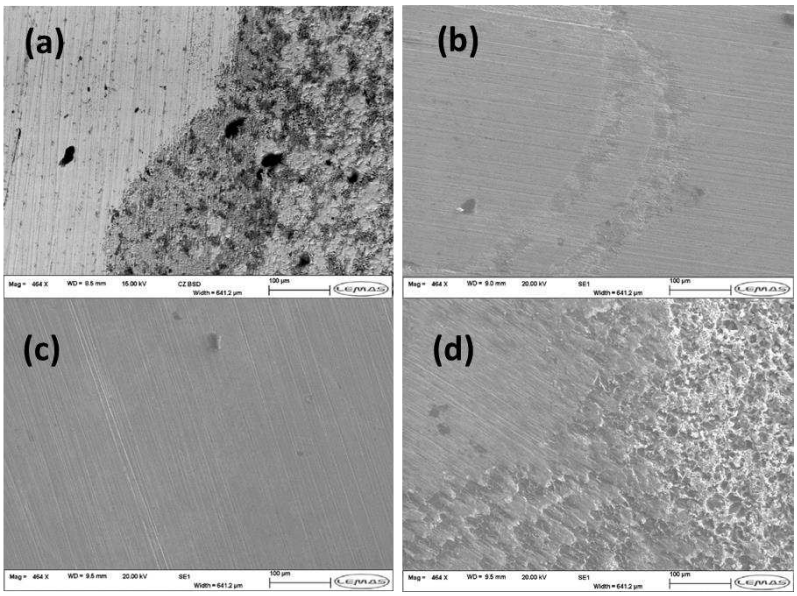

Figure 14: SEM for X65 after exposure 80°C 3 wt. % NaCl brine saturated with CO_2 for 48 h with 30 ppm imidazoline based corrosion inhibitor aged for (a) 0 h, (b) 24 h, (c) 48 h and (d) 120 h at 80°C.

SEM analysis of the steel surfaces (Fig. 14) confirmed that the specimens exposed to the 24 and 48 h aged inhibitors experienced very little corrosion, creating surfaces which were smoother than for the non-aged inhibitor (Fig. 14, b and c). The specimen exposed to the 120 h aged imidazoline inhibitor (Fig. 16, d) appeared to be more corroded with a visually rougher surface. These findings are consistent with electrochemistry data in Fig. 12.

The end-point (η_{End}) and integrated (η_{Int}) inhibition efficiencies of the aged inhibitors are plotted as a function of inhibitor aging time in Fig. 15 (a). The polarization resistance was used to calculate the end-point and integrated corrosion inhibitor efficiencies:

$$\eta_{End}(\%) = \left[1 - \left(\frac{R_{P,Uninhibited}}{R_{P,Inhibited}}\right)\right] \times 100 \qquad (3)$$

$$\eta_{Int}(\%) = \left[1 - \left(\frac{R_{P,Uninhibited}}{\int_0^{48} R_{P,Inhibited}}\right) dt\right] * 100 \qquad (4)$$

where $R_{P,Inhibited}$ is the polarization resistance at the end of the inhibited corrosion experiment (ohm.cm²) and $R_{P,Uninhibited}$ is the polarization resistance in the uninhibited corrosion test (ohm.cm²).

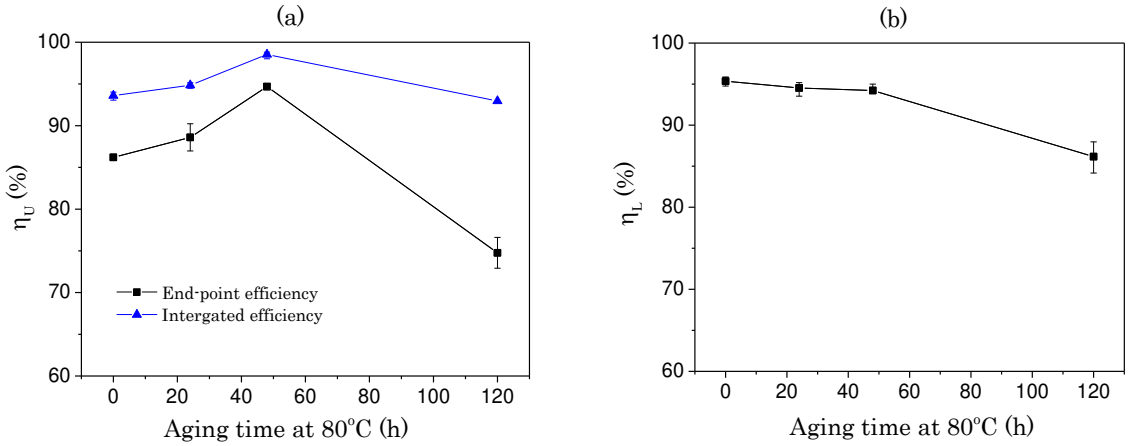

Figure 15: The effect of aging time at 80°C of imidazoline based corrosion inhibitor on uniform, η_U (a) and localized, η_L (b) inhibitor efficiency for X65 at 80°C in 3 wt. % NaCl brine saturated with CO_2

We observe that both end-point, η_{End} and integrated, η_{Int} uniform inhibition efficiency, η_U increases after pre-aging the inhibitor for 24 and 48 h but then inhibition efficiency decreases when the inhibitor is pre-aged for 120 h. However, although aging of the inhibitor for 24 and 48 h led to improved performance with respect to generalised corrosion, the same trend was not observed with respect to localized corrosion (Fig. 15, b). The localized efficiency of the corrosion inhibitor was determined using the change in pit depth. The maximum pit depths observed in the absence and presence of the non-aged inhibitor were 26.1 and 1.2 µm respectively. Increasing the inhibitor aging time at 80°C (Fig. 15, b) resulted in the formation of deeper pits on the steel surface which led to a decrease in the localized inhibitor efficiency from 95.4% for fresh inhibitor to 94.5 (1.4 µm), 94.2% (1.51 µm) and 86.1% (3.6 µm) for the inhibitor aged for 24, 48 and 120 h, respectively.

3.3.2 Aging at 120°C

The imidazoline inhibitor was aged at its thermal stability limit at 120°C for 2, 6 and 24 h followed by performance testing at 80°C in order to evaluate its performance after partial

hydrolysis of the corrosion inhibitor. All the 120°C aged inhibitor products showed reduced inhibition performance (Fig. 16, a and Table 3) such that the stabilised $1/R_p$ increases with increasing inhibitor aging time. These results suggest that pre-aging the inhibitor at 120°C results in extensive hydrolysis of the inhibitor structure resulting in degradation of the inhibitor performance. These findings are consistent with those of Ding *et al* [31] who observed a 40-50% loss of corrosion inhibitor performance due to hydrolysis when testing at 120 and 150°C.

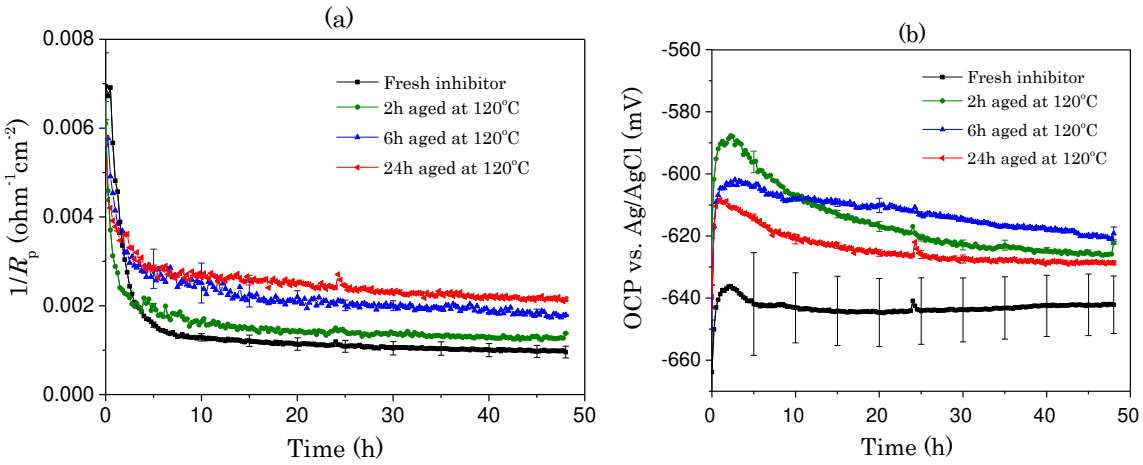

Figure 16: Reciprocal of polarization resistance (a) and OCP (b) versus exposure time for X65 at 80°C in CO_2 saturated 3 wt. % NaCl brine with 30 ppm imidazoline based corrosion inhibitor pre-aged for 0, 2, 6 and 24 h at 120°C.

Table 3: Corrosion rate versus exposure time for X65 at 80°C in CO_2 saturated 3 wt. % NaCl brine with 30 ppm imidazoline based corrosion inhibitor pre-aged for 0, 2, 6 and 24 h at 120°C.

	Corrosion rate (mm/year)			
Time (h)	**Fresh inhibitor**	**Aged 2 h**	**Aged 6 h**	**Aged 24 h**
0	1.15	1.01	0.93	0.94
1	0.80	0.47	0.68	0.62
2	0.50	0.37	0.53	0.60
5	0.26	0.33	0.47	0.47
10	0.21	0.27	0.41	0.44
24	0.19	0.24	0.33	0.40
48	0.15	0.22	0.29	0.35

pH measurements of the bulk solution during testing the inhibitors pre-aged at 120°C (Fig. 17) indicate that the longer the inhibitor is pre-aged the greater is the increase in pH during the 0-48 h period (due to higher corrosion). This trend is consistent with the order of the reciprocal of the polarization resistances measured after 48 h exposure (Fig. 16).

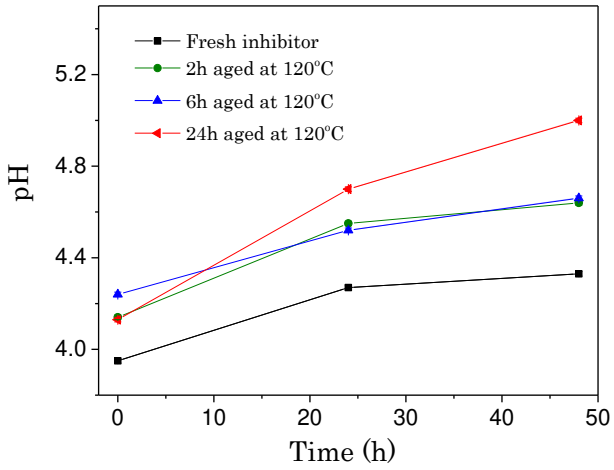

Figure 17: Brine pH at 80°C for X65 in 3 wt. % NaCl brine saturated with CO_2 with 30 ppm imidazoline based corrosion inhibitor pre-aged for 0, 2, 6 and 24 h at 120°C.

SEM analysis of the carbon steel specimens (Fig. 18) indicated that all the specimens had two distinct areas, one of which was more heavily corroded than the other. In all cases, the lightly corroded areas corresponded to the majority of the surface area and the heavily corroded zones constituted the minority of the surface area. All specimens exposed to the 120°C aged inhibitors contained a visibly more severely corroded area than the corroded area of the specimen exposed to the non-aged inhibitor. The SEM top-view images also revealed that the extent of corrosion in the lighter and heavier corroded zones increased with increasing aging time.

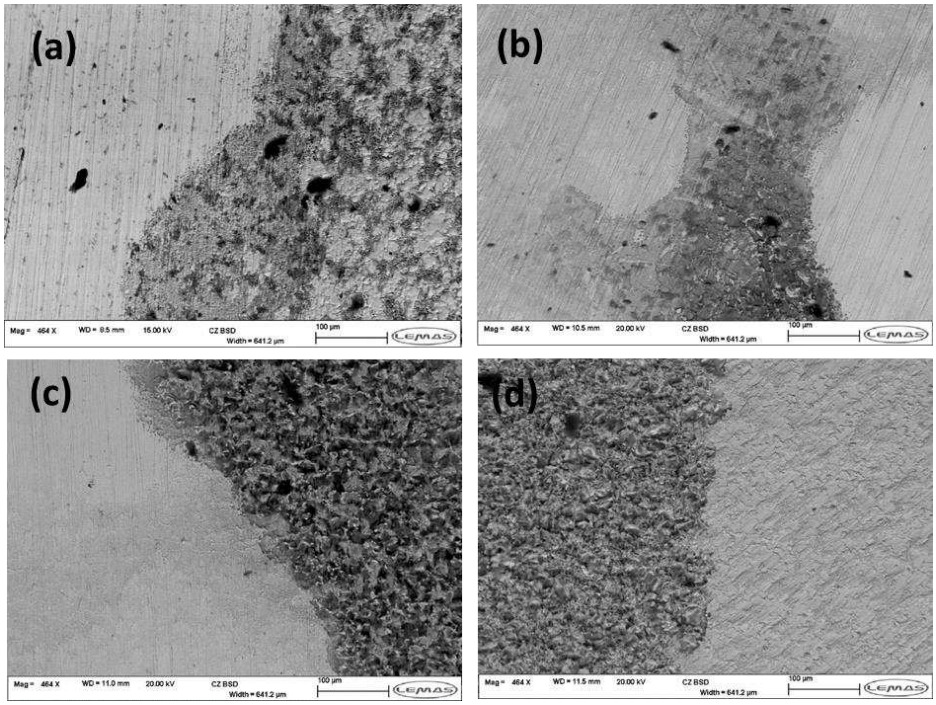

Figure 18: SEM for X65 after exposure 80°C 3 wt. % NaCl brine saturated with CO_2 for 48 h with 30 ppm imidazoline based corrosion inhibitor aged for (a) 0 h, (b) 2 h, (c) 6 h and (d) 24 h at 120˚C.

Inhibitor efficiency calculations of the 120°C aged inhibitor tests (Fig. 19, a) revealed that the uniform inhibitor efficiency decreased more steeply with increasing pre-aging time as compared to the inhibitor aged at 80°C (Fig. 15). This is consistent with the expected effect of temperature on the rate of hydrolysis, where, its rate increases exponentially with increasing temperature (Fig. 10, 11). The decrease in inhibitor performance with respect to generalised corrosion was accompanied by a large decrease in performance with respect to localized corrosion (Fig. 19, b). The localized corrosion inhibitor efficiency was reduced from 95.4 (1.2 μm) to ~73% (7 μm) for the imidazoline inhibitor aged at 120°C for 6 h and 24 h. These findings confirm that a reduction in the imidazoline **1** and amido-amine **2** concentration as well as further amido-amine **2** hydrolysis via second step, may be a contributing factor to its poor performance however more importantly demonstrating its detrimental effect on its ability in preventing localized corrosion attack.

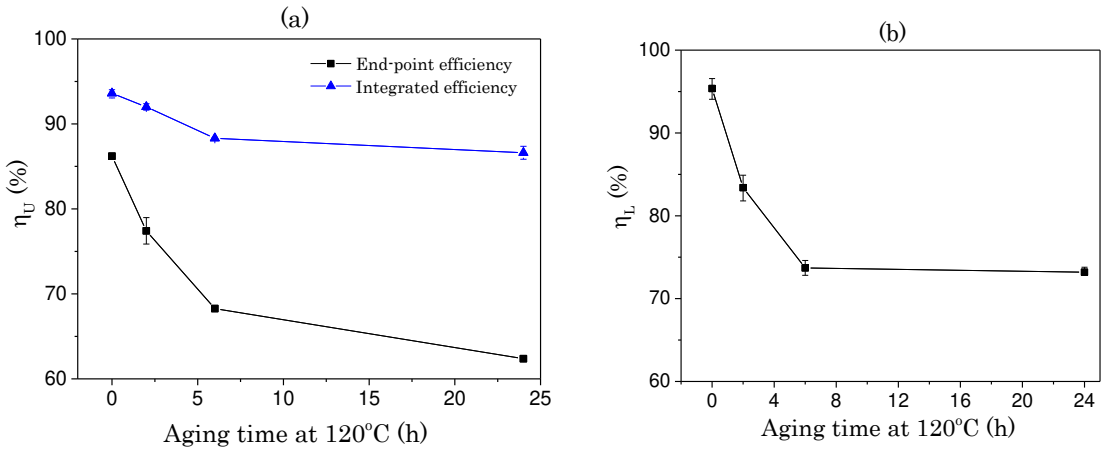

Figure 19: The effect of aging time at 120°C of imidazoline based corrosion inhibitor on uniform, η_U (a) and localized, η_L (b) inhibitor efficiency for X65 at 80°C in 3 wt. % NaCl brine saturated with CO_2

4.0 Conclusions

This paper investigates the molecular characteristics of a TOFA/DETA imidazoline based corrosion inhibitor (reaction blend of imidazoline **1** and its precursor, amido-amine **2**), the rate of its acid catalysed hydrolysis in CO_2 saturated 3 wt. % NaCl at 70 – 120C°, and the corrosion performance of fresh inhibitor and the products of its hydrolysis for wet-ground X65 carbon steel in CO_2 saturated 3 wt. % NaCl brine at 80°C with regard to uniform/localized corrosion. We conclude:

1) The imidazoline based corrosion inhibitor forms micellar solutions and the characteristic micelle size in a CO_2 saturated 3 wt. % NaCl brine at the CMC concentration, 10±1 ppm (~29 μM), is 18±9 nm. A change in the concentration of the inhibitor in the range from 10 to 1000 ppm and in the pH of the solution (from pH 4.1 to 5.6) does not significantly affect the micelle size. Potentiometric titration data show that the imidazoline based inhibitor has two equivalency points at pH 9.2 and pH 4.8 suggesting that, under CO_2 saturated 3 wt. % NaCl (pH~4.1) conditions, the inhibitor is fully protonated. Such protonation increases inhibitor solubility/dispersibility in brine and enhances molecular adsorption of the positively charged imidazoline on the metal surface thereby improving inhibition performance.

2) ATR FTIR spectroscopy was used to determine the hydrolysis constant and composition of aged corrosion inhibitor. The ratio of the absorbance of the characteristic bands due to imidazoline **1** and amido-amine **2**, Abs 1607 cm^{-1}/ Abs 1646 cm^{-1}, was used to monitor the *relative* quantities of imidazoline **1** and amido-amine **2** in aged inhibitor solution in CO_2 saturated 3 wt. % NaCl at pH~4.1. The hydrolysis of imidazoline **1** and amido-amine **2** is

catalysed by acid and the consumption of imidazoline **1** follows a pseudo-first-order reaction mechanism with activation energy of 72.0±2.9 kJ mol^{-1}.

3) Pre-aging the imidazoline based inhibitor in CO_2 saturated 3 wt. % NaCl brine at 80°C has different effects on the uniform and localized corrosion behavior of X65 carbon steel. The localized, η_L inhibitor efficiency decreases over time, which is caused by a decrease in the concentration of the inhibitor in the system, which is very sensitive to the concentration of the inhibitor when it drops below 30 ppm [12]. In contrast, aging of the inhibitor at 80°C for 24 and 48 h increases the uniform inhibition efficiency, η_U due to an increase in the relative amount of amido-amine **2** in the composition of the degraded inhibitor. Adsorption of the more hydrophobic and less soluble amido-amine **2** precursor on metal surface has some positive effect on inhibitory performance. However, an increase in degradation time, 120 h at 80°C, or aging temperature, 120°C, decreases the total concentration of the inhibitor in solution, mainly due to hydrolysis of the imidazoline based inhibitor via a second step mechanism; this decreases inhibition efficiency, η_U since the end products of hydrolysis, i.e. DETA **3** and TOFA **4** are very poor inhibitors.

5.0 Data availability

The raw/processed data required to reproduce these findings cannot be shared at this time as the data also forms part of an ongoing study.

6.0 References

1. M. A. J. Mazumder, H. A. Al-Muallem, S. A. Ali, Corros. Sci. (2015) 54-68
2. M. A. J. Mazumder, M. K. Nazal, M. Faiz, S. A. Ali, Imidazolines containing single-, twin- and triple-tailed hydrophobes and hydrophilic pendants $(CH_2CH_2NH)_nH$ as inhibitors of mild steel corrosion in CO2–0.5 M NaCl, RSC Advances (2016) 12348-12362.
3. J. Zhang, J. Liu, W. Yu, Y. You, L. Liu, Molecular modeling of the inhibition mechanism of 1-(2-aminoethyl)-2-alkyl-imidazoline, Corros. Sci. (2010) 2059-2065.
4. S. Ramachandran,B.-L. Tsai, M. Blanco, H. Chen, Y. Tang, W. A. Goddard, Self-assembled monolayer mechanism for corrosion inhibition of iron by imidazolines, Langmuir (1996) 6419-6428.
5. S.-H. Yoo, Y-W. Kim, K. Chung, S.-Y. Baik, J.-S. Kim, Synthesis and corrosion inhibition behavior of imidazoline derivatives based on vegetable oil, Corros. Sci. (2012) 42-52.
6. J. Porcayo-Calderon , I. Regla, E. Vazquez-Velez, L. M. Martinez de la Escalera, J. Canto, M. Casales-Diaz, Effect of the unsaturation of the hydrocarbon chain of fatty-amides on the CO_2 corrosion of carbon steel using EIS and real-time corrosion measurement, Spectroscopy (2015) ID 184140.

7. H. J. Chen, W. P. Jepson, T. Hong, High temperature corrosion inhibition performance of imidazoline and amide, NACE Conference (2000) 00035.
8. S. Ramachandran, C. Menendez, V, Jovancicevic, J. Long, Film persistency of new high-temperature water-based batch corrosion inhibitors for oil and gas wells, J. Petrol. Explor. Prod. Technol. (2012), 25-131.
9. Y. Xiong, B. Brown, B. Kinsella, S. Nešic, A. Pailleret, Atomic force microscopy study of the adsorption of surfactant corrosion inhibitor films, Corros. (2014) 247-260.
10. M. A. Gough, W. H. Durnie, E. K. Auty, B. Hedges, Characterization, isolation and performance characteristics of imidazolines, Corros. (2002) 02301.
11. W. Durnie, M. Gough, Characterization, Isolation and performance characteristics of imidazolines: Part II development of structure-activity relationships, Corros. (2003) 03336.
12. A. Shamsa, R. Barker, Y. Hua, E. Barmatov, T. Hughes, A. Neville, Performance evaluation of an imidazoline corrosion inhibitor in a CO2-saturated environment with emphasis on localized corrosion, Corros. Sci. (2020) 108916.
13. J. A. Martin, F. W. Valone, The existence of imidazoline corrosion inhibitors, Corros. (1985) 281-287.
14. B. J. Usman, S. A. Ali, Carbon Dioxide Corrosion Inhibitors: A review, Arab. J. Sci. Eng. (2018) 1-22.
15. J. A. Martin, F. W. Valone, Spectroscopic techniques for quality assurance of oil field corrosion inhibitors, Corrosion (1985) 465-743.
16. D. Bajpai, V. Tyagi, Fatty Imidazolines: Chemistry, Synthesis, Properties and Their Industrial Applications. J. Oleo Sci. (2006) 319-329.
17. R. Tyagi, V. K. Tyagi, S. K. Pandey, J. Oleo Sci. (2007) 211-222.
18. S. Bondareva, Y. Murinov, L. Spirikhin, Protonation of 1,2-disubstituted imidazolines and other products of condensation of 2-ethylhexanoic acid with diethylenetriamine and triethylenetetramine, Russ. Chem. Bull. (2000) 2007-2012.
19. K. Kousar, T. Ljungdahl, A. Wetzel, M. Dowhyj, H. Oskarsson, A. S. Walton, M. S. Walczak, R. Lindsay, An exemplar imidazoline surfactant for corrosion inhibitor studies: synthesis, characterisation and physicochemical properties, J. Surfact. Deterg. (2019) 225-234.
20. Chemaxon. (2019) Chemicalize. Retrieved from https://chemicalize.org
21. M. Zhao, H. He, C. Dai, X. Wu, Y. Zhang, Y. Huang, C. Gu, Micelle formation by amine-based CO2-responsive surfactant of imidazoline type in an aqueous solution, J. Mol. Liq. (2018) 875-888.

22. A. Khoshnood, B. Lukanov, A. Firoozabadi, Temperature effect on micelle formation: molecular thermodynamic model revisited, Langmuir 2016, 2175-2183.
23. Wei Li, B.F.M. Pots, Xiankang Zhong, Srdjan Nesic, Inhibition of CO_2 corrosion of mild steel – Study of mechanical effects of highly turbulent disturbed flow, Corros. Sci. (2017) 208-226.
24. M. W. S. Jawich, G. A. Oweimreen, S. A. Ali, Heptadecyl-tailed mono- and bis-imidazolines: A study of the newly synthesized compounds on the inhibition of mild steel corrosion in a carbon dioxide-saturated saline medium, Corros. Sci. (2012) 104-112.
25. M. M. Watts, Imidazoline Hydrolysis in alkaline and acidic media - a review, JAOCS (1990), 993-995.
26. B. G. Harnsberger, J. L. Riebsomer, The kinetics of the hydrolysis of some 2-imidazolines, J. Heterocyclic Chem. (1964) 229-232.
27. S. O. Bondareva, V. V. Lisitskii, N. I. Yakovtseva, Yu. I. Murinov, Hydrolysis of 1,2-disubstituted imidazolines in aqueous media, Russ. Chem. Bull., Int. Ed. (2004) 803-807.
28. B. G. Harnsberger, J. L. Riebsomer, The influence of alkyl substituents on the rates of hydrolysis of 2-imidazolines, J. Heterocyclic Chem. (1964) 188-192.
29. A. Savignac, T. Kabbage, P. Dupin, and M. Calmon, Etude cinétique de l'ouverture du cycle Δ2 imidazoline par hydrolyse basique, J. Heterocycl. Chem. (1978) 897.
30. A. Jenkins, Performance of High-Temperature, Biodegradable Corrosion Inhibitors. Corros. (2011) 11272.
31. Y. Ding, B. Brown, D. Young and M. Singer, Effectiveness of an imidazoline-type inhibitor against CO_2 corrosion of mild steel at elevated temperatures (120°C-150°C), Corros. (2018), 11622.